Open access • Journal Article • DOI:10.1088/0266-5611/10/2/008

An image-enhancement technique for electrical impedance tomography

David C. Dobson, Fadil Santosa

Institutions: University of Minnesota, University of Delaware

Published on: 01 Apr 1994 - Inverse Problems (IOP Publishing)

Topics: Electrical impedance tomography, Inverse problem, Image processing and Piecewise

AN IMAGE ENHANCEMENT TECHNIQUE FOR ELECTRICAL IMPEDANCE TOMOGRAPHY

By

David C. Dobson

and

Fadil Santosa

IMA Preprint Series # 1145

June 1993

AN IMAGE ENHANCEMENT TECHNIQUE FOR ELECTRICAL IMPEDANCE TOMOGRAPHY*

DAVID C. DOBSON† AND FADIL SANTOSA‡

Abstract. In this paper, we propose an idea for reconstructing "blocky" conductivity profiles in electrical impedance tomography. By "blocky" profiles, we mean functions that are piecewise constant, and hence have sharply defined edges. The method is based on selecting a conductivity distribution that has the least total variation from all conductivities that are consistent with the measured data. We provide some motivation for this approach and formulate a computationally feasible problem for the linearized version of the impedance tomography problem. A simple gradient descent-type minimization algorithm, closely related to recent work on noise removal in image processing via nonlinear diffusion is described. The potential of the method is demonstrated in several numerical experiments.

Key Words. elliptic inverse problem, electrical impedance tomography, conductivity imaging, image enhancement, edge detection, minimal total variation

AMS(MOS) subject classifications. 35R30

1. Introduction. The goal in electrical impedance tomography is to find a spatially varying conductivity distribution inside a given domain, given electrostatic measurements collected at the boundary. This problem has numerous practical applications, for example in medical imaging [3].

The idealized model problem can be stated as follows. Given some domain $\Omega \subset \mathbb{R}^p$, $p = 2$ or 3, the problem is to find the conductivity distribution in the interior of Ω from electrostatic measurements on the boundary $\partial\Omega$. A spatially distributed current flux density pattern f which satisfies $\int_{\partial\Omega} f = 0$ is applied to $\partial\Omega$. The voltage potential u inside Ω then satisfies

$$\nabla \cdot (\sigma \nabla u) = 0 \quad \text{in } \Omega, \tag{1a}$$

where σ is the conductivity of the medium, with the Neumann boundary condition

$$\sigma \frac{\partial u}{\partial \nu} = f \quad \text{on } \partial\Omega. \tag{1b}$$

With the additional normalization constraint $\int_{\partial\Omega} u = 0$, and the assumption that σ is uniformly bounded away from zero, equations (1) uniquely determine the voltage potential u in appropriate function spaces.

For every "current pattern" f, we measure the corresponding voltage potential u on the boundary $\partial\Omega$. Hence, the data in the problem can be viewed as the so-called Neumann-to-Dirichlet map $F(\sigma; f)$ which takes current patterns to voltage measurements, defined by $F(\sigma; f) = u|_{\partial\Omega}$, where u satisfies (1). Note that F is linear in the second variable but nonlinear in the first variable.

In practice, one is limited to performing only a finite set of experiments, generally carried out with f in some finite-dimensional space such as that spanned by a given

* This work is supported by the National Science Foundation and the Air Force Office of Scientific Research. The first author is supported by an NSF Mathematical Sciences Postdoctoral Fellowship.

† School of Mathematics, University of Minnesota, Minneapolis, MN 55455-0436 dobson@ima.umn.edu

‡ Department of Mathematical Sciences, University of Delaware, Newark, DE 19716 santosa@math.udel.edu

number of electrodes in fixed positions. In addition, of course, it is infeasible in practice to measure all of $u|_{\partial\Omega}$; one is left with samples of u at a finite number of points on the boundary $\partial\Omega$. Obviously, given a finite amount of data, the practical problem of determining σ (which in principle has an infinite number of unknowns) is impossible. In fact, even after approximating σ in a finite dimensional space of reasonably small dimension, experience and analysis indicate that one is generally left with an extremely unstable problem. This is to be expected since the underlying inverse problem is ill-posed.

The instability of the inverse problem renders the practical task of reconstructing conductivity profiles very difficult. This instability has been characterized in various ways by studying the linearized problem [1, 6, 8]. The main difficulty is that the measured data are very insensitive to certain features in the conductivity profile. For instance, two profiles that differ primarily in the high-frequency Fourier components may yield boundary data that are nearly indistinguishable. Such behaviors are manifestations of the information content of the data: information about abrupt changes in the conductivity profile is not contained in the measured data. Therefore any reconstruction procedure will be unstable to data errors unless the problem is properly regularized. The main consequence of regularization is that conductivity images are often smeared, blurred, or distorted in the reconstruction.

The central idea in this paper is that we incorporate *a priori* information about the unknown conductivity. The *a priori* information is roughly the knowledge that the unknown conductivity is "blocky" in nature. By "blocky" we mean that the conductivity is a piecewise constant function, and thus has sharp edges. We show that the "blockiness" attribute can be characterized by the total variation of the conductivity. Thus, our approach can be described as the problem of finding the minimal total variation conductivity, which we formulate as an optimization problem. Our optimization strategy generates a sequence of conductivities with decreasing total variation, all of which satisfy the constraints imposed by the measured data.

Measuring the total variation has long been recognized as an effective way to quantify the "simplicity" of a given signal or function. It has the advantage that it measures the "oscillations" of a given function, but it does not unduly punish discontinuities. The strategy of finding minimal total variation reconstructions and, more generally, the "nonlinear diffusion approach", has proved successful in applications such as image processing [14, 13, 2, 4], optimal design [7], and seismic inverse problems [15, 16].

In [14], Rudin, Osher, and Fatemi describe a method for image recovery from noisy data. Our method is essentially based on the ideas presented in [14]. In order to apply it to our problem, we had to devise a way to handle the unstable constraints imposed by the underlying inverse problem. We assume that the conductivity is a piecewise constant function on a square array of square pixels, which allows us to compute its total variation *exactly*. We also introduce a mollification of the objective functional in order to implement a step-length selection procedure in the minimization. The strategy in some sense solves an underlying nonlinear elliptic boundary value problem which appears as the Euler-Lagrange equations for the constrained minimization. The minimization procedure we adopt can be viewed as the time evolution of a function whose steady state is described by the nonlinear elliptic boundary value problem. It is interesting to note that the method is closely related to the problem of evolving surfaces by their mean curvature.

The paper is organized into 7 sections. We motivate our approach in Section 2,

wherein we also describe the optimization problem we must consider. This is followed by a demonstration that the problem, formulated as a constrained optimization, admits a solution. In Section 4 we propose a strategy for stabilizing the constraints imposed by the data. Section 5 is devoted to the minimization method. In Section 6, we show an implementation of our method and demonstrate its potential in several numerical examples. A final section contains a discussion on future research directions.

2. The linearized problem and the minimal total variation approach. For the sake of definiteness, let us henceforth assume that the domain Ω is the unit disk in $\mathbb{R}^2$. We emphasize that our techniques are still valid in more complicated geometries. In polar coordinates, we set $\Omega = \{(r,\theta) : r < 1\}$, and $\partial\Omega = \{(r,\theta) : r = 1\}$. Furthermore, we make the practical assumption that the current patterns f are generated by a finite number n of fixed electrodes. Thus, we write f in the form

$$f(\theta) = \sum_{i=1}^{n} f_i \chi(\theta, \theta_i), \tag{2}$$

where χ is the characteristic function

$$\chi(\theta,\theta_i) = \begin{cases} 1/h & \text{for} \quad |\theta - \theta_i| \le h/2, \\ 0 & \text{otherwise,} \end{cases}$$

h is the electrode width, and $\{\theta_i\}_{i=1}^n$ are the electrode centers. We identify the current pattern "function" f with the n-vector $(f_i)_{i=1}^n$. Finally, we assume that our measurements are taken as voltage drops between adjacent electrodes. That is, let u_i be the voltage potential at electrode i, then the data, corresponding to a current pattern f, is the $\mathbb{R}^n$ vector

$$g = (g_1, g_2, \cdots, g_n)^T,$$

where $g_i = u_{i+1} - u_i$ (and electrode $n+1$ is identified with electrode 1). The forward map $F(\sigma, f)$ is viewed as taking a current pattern $f \in \mathbb{R}^n$ and a conductivity distribution σ to an $\mathbb{R}^n$ vector; the ith component of the map is

$$(F(\sigma,f))_i = u(1,\theta_{i+1}) - u(1,\theta_i).$$

If we make n measurements, that is, we apply n different current patterns

$$f^{(1)}, f^{(2)}, \ldots, f^{(n)},$$

and measure the corresponding voltage drops

$$g^{(1)}, g^{(2)}, \ldots, g^{(n)},$$

then the (nonlinear) inverse problem is to determine σ such that

$$F(\sigma; f^{(j)}) = g^{(j)}, \quad j = 1, \ldots, n.$$

A common technique to simplify the analysis of the problem, which we adopt in this work, is to linearize F by assuming that the conductivity is some small perturbation about a constant background. Thus, we let

$$\sigma = 1 + \delta\sigma$$

where the function $\delta\sigma$ is "small", and assume that the voltage potential is

$$u = U + \delta u.$$

By considering terms of the same order in (1a), we see that the background potential U satisfies

$$\triangle U = 0 \quad \text{in } \Omega, \tag{3a}$$

$$\frac{\partial U}{\partial \nu} = f \quad \text{on } \partial\Omega, \tag{3b}$$

where f is given in (2). We still impose the normalization condition $\int_{\partial\Omega} U = 0$. The perturbational voltage potential δu satisfies

$$\triangle \delta u = -\nabla \cdot \delta\sigma \nabla U \quad \text{in } \Omega, \tag{4a}$$

$$\frac{\partial \delta u}{\partial \nu} = 0 \quad \text{on } \partial\Omega, \tag{4b}$$

where we again enforce the normalization $\int_{\partial\Omega} \delta u = 0$. Since U depends linearly on the current pattern f, we see that δu is also linearly dependent on f.

For a given current pattern f, the linearized forward map DF takes a conductivity perturbation $\delta\sigma$ to perturbational measurements on the boundary. The i-th component of this map is

$$(DF(f)\delta\sigma)_i := \delta u(1, \theta_{i+1}) - \delta u(1, \theta_i). \tag{5}$$

Assuming that $\delta\sigma$ is supported in $\Omega' = \{r \leq r' < 1\}$, we can view the map as

$$DF(f) : L^1(\Omega') \to I\!R^n. \tag{6}$$

Defining appropriate generalized solutions of problem (4a) and using elliptic regularity (see e.g. [10]), it is easy to show that $DF(f)$ is well-defined and bounded over $L^1(\Omega')$. We shall extend the domain of DF to $L^1(\Omega)$ by cutting off perturbations whose support lies outside of Ω', i.e.

$$DF(f) : L^1(\Omega) \to I\!R^n \tag{7}$$

is defined by $DF(f)\delta\sigma := DF(f)(\chi_{\Omega'}\delta\sigma)$ where $\chi_{\Omega'}$ is the characteristic function on Ω'.

In the linearized inverse problem, the goal is to find $\delta\sigma$ from knowledge of the *differences* between the measured voltage drops and the background voltage drops $U(1, \theta_{i+1}) - U(1, \theta_i)$ for a set of current patterns $f^{(j)}$, $j = 1, \cdots, n$. Let us denote the background voltage due to current pattern $f^{(j)}$ by $U^{(j)}$. The linearized inverse problem is to determine $\delta\sigma$ in the equation

$$DF(f^{(j)})\delta\sigma = g^{(j)} - TU^{(j)} =: \delta g^{(j)}, \quad \text{for} \quad j = 1, \cdots, n, \tag{8}$$

where $TU^{(j)}$ is the $I\!R^n$-vector whose components are $(U^{(j)}(1, \theta_{i+1}) - U^{(j)}(1, \theta_i))$. To simplify notation, let us assume that the current patterns $f^{(1)}, \ldots, f^{(n)}$ have been chosen and are henceforth *fixed*. Forming the $I\!R^{n^2}$ data vector

$$\delta g = (\delta g^{(1)T}, \ldots, \delta g^{(n)T})^T$$

and the corresponding operator

$$DF = (DF(f^{(1)})^T, \ldots, DF(f^{(n)})^T)^T,$$

we can then state the linearized inverse problem

$$DF\ \delta\sigma = \delta g. \tag{9}$$

Again, $\delta\sigma$ is clearly not determined because of lack of data. Moreover, as stated in the Introduction, even if we discretize the problem to a finite number of unknowns in $\delta\sigma$, the conductivity perturbation $\delta\sigma$ is generally not well-determined by the data due to lack of continuity of the conductivity-to-data relation [1, 6, 8]. In particular, information corresponding to high frequency components of $\delta\sigma$ is lost in the data.

Our approach to increase resolution is to incorporate *a priori* information about the conductivity perturbation $\delta\sigma$ in the problem. We assume that the unknown $\delta\sigma$ is "blocky"; i.e., it is piecewise constant. Therefore the assumption that the true conductivity perturbation can be described as a sum of characteristic functions:

$$\delta\sigma(x) = \sum_{k=1}^{N} a_k \chi(\Omega_k)(x) \tag{10}$$

is justified. Here N is unknown but finite, the coefficients a_k are unknown, the subdomains $\Omega_k \subset\subset \Omega$ are unknown, and $\chi(\Omega_k)$ denotes the characteristic function on Ω_k. For convenience, assume that each Ω_k has a C^2 boundary $\partial\Omega_k$. Equation (10) represents a very wide variety of conductivity profiles which may be encountered in applications ranging from medical imaging to non-destructive testing.

Let $\nabla\delta\sigma$ denote the gradient of $\delta\sigma$ in the sense of distributions; $\nabla\delta\sigma$ is a vector valued Radon measure and

$$\int_\Omega |\nabla\delta\sigma| \tag{11}$$

is the total variation of $\delta\sigma$. We denote by $BV(\Omega)$ the space of functions of bounded variation in Ω, equipped with the norm

$$\|\delta\sigma\|_{BV(\Omega)} = \|\delta\sigma\|_{L^1(\Omega)} + \int_\Omega |\nabla\delta\sigma|$$

(see for example [11]). We observe that $\delta\sigma$ defined by (10) is in $BV(\Omega)$.

Now suppose that we are trying to reconstruct $\delta\sigma$, but due to the ill-posedness of the problem, we are only able to obtain an approximation $\widetilde{\delta\sigma}$, and $\widetilde{\delta\sigma} = \delta\sigma + \eta$, where η is some unknown "error" component. In practice, $\widetilde{\delta\sigma}$ is often a blurred version of $\delta\sigma$. We assert that if η is relatively well-behaved, then

$$\int_\Omega |\nabla(\delta\sigma + \eta)| \geq \int_\Omega |\nabla\delta\sigma|,$$

which suggests that in order to recover $\delta\sigma$, we must find η such that $\widetilde{\delta\sigma}$ has the least total variation.

In fact, we can make the following statement.

PROPOSITION 2.1. *Suppose that $\delta\sigma$ is given by (10) and $\eta \in W^{1,1}(\Omega)$. Then*

$$\int_\Omega |\nabla(\delta\sigma + \eta)| = \int_\Omega |\nabla\delta\sigma| + \int_\Omega |\nabla\eta|, \tag{12}$$

where the derivatives are interpreted in the sense of distributions.

Proof. Let ϕ_ϵ be a smooth mollifier function supported in a ball of radius ϵ; denote the convolution $\delta\sigma_\epsilon = \delta\sigma * \phi_\epsilon$. Then $\nabla\delta\sigma_\epsilon$ is a smooth function supported in an ϵ-neighborhood B_ϵ of the set $B = \cup_{k=1}^{N} \partial\Omega_k$ and

$$\int_\Omega |\nabla(\delta\sigma_\epsilon + \eta)| = \int_{B_\epsilon} |\nabla\delta\sigma_\epsilon + \nabla\eta| + \int_{\Omega - B_\epsilon} |\nabla\eta|.$$

From the estimate

$$\int_\Omega |\nabla\delta\sigma_\epsilon| - \int_{B_\epsilon} |\nabla\eta| \leq \int_{B_\epsilon} |\nabla\delta\sigma_\epsilon + \nabla\eta| \leq \int_\Omega |\nabla\delta\sigma_\epsilon| + \int_{B_\epsilon} |\nabla\eta|$$

and the Lebesgue Dominated Convergence Theorem, we see that

$$\lim_{\epsilon\to 0} \int_\Omega |\nabla(\delta\sigma_\epsilon + \eta)| = \lim_{\epsilon\to 0} \int_\Omega |\nabla\delta\sigma_\epsilon| + \int_\Omega |\nabla\eta|.$$

The equality (12) then follows from elementary properties of convergence in $BV(\Omega)$ (see [11]). □

We mention that Proposition 2.1 can be generalized to include slightly larger classes of $\delta\sigma$ and η. However, since our intention here is only to try to motivate our approach, we will keep this simple version.

Proposition 2.1 suggests that if the "error" component of the reconstructed conductivity perturbation $\delta\tilde{\sigma}$ is relatively smooth, then we *can*, in general, recover $\delta\sigma$ simply by looking for η which makes $\delta\tilde{\sigma}$ have the least total variation. This can be posed as an optimization problem

$$\min_{\delta\sigma\in\mathcal{A}} \int_\Omega |\nabla\delta\sigma|, \tag{13a}$$

$$\text{subject to: } DF\delta\sigma = \delta g, \tag{13b}$$

where $\mathcal{A}$ is some admissible class of conductivity perturbations. The constraint ensures that all feasible conductivity perturbations match the observed data.

It is difficult to estimate a priori that the error η committed in the reconstruction must belong to $W^{1,1}(\Omega)$; otherwise we could guarantee exact reconstructions of conductivities in the form (10) by finding the minimal total variation reconstruction. Nevertheless, experience indicates that reconstruction errors often have a large "smooth" component and this provides some motivation for our approach.

Proposition 2.1 is similar in spirit to an estimate made by Santosa and Symes [15, 16] in the discrete one-dimensional case. Their work was in the context of inverting band-limited reflection seismograms. Donoho [9] has carried out extensive analysis on the closely related problem of "superresolving" discrete signals from band-limited data.

3. Existence of a minimizer. The minimal total variation reconstruction problem (13) can be written

$$\min_{\delta\sigma\in X} J(\delta\sigma) = \int_\Omega |\nabla\delta\sigma|, \tag{14a}$$

$$\text{subject to } DF\ \delta\sigma = \delta g, \tag{14b}$$

where $X = \{\delta\sigma \in BV(\Omega) : \delta\sigma|_{\partial\Omega} = 0\}$. Since J is a convex functional and the constraints are linear, any local minimizer of problem (14) must be a global minimizer. However, since J is not *strictly* convex, uniqueness of solutions is doubtful.

Since DF is well-defined and bounded over $L^1(\Omega)$, we can define the set

$$Y = \{\delta\sigma \in BV(\Omega) : \delta\sigma|_{\partial\Omega} = 0, \quad DF\ \delta\sigma = \delta g\}.$$

The minimization problem (14) can then be equivalently written

$$\min_{\delta\sigma \in Y} J(\delta\sigma). \tag{15}$$

THEOREM 3.1. *Given any data vector $\delta g \in \mathbb{R}^{n^2}$ in the range of DF, the problem (15) admits at least one solution $\delta\sigma \in BV(\Omega)$.*

To prove the theorem, we use the following fundamental compactness result. See [11] for a proof.

LEMMA 3.2. *Given $K < \infty$, the set*

$$\{\delta\sigma \in BV(\Omega) : \|\delta\sigma\|_{BV(\Omega)} \leq K\}$$

is compact in $L^1(\Omega)$. Furthermore, if $\delta\sigma_k \rightarrow \delta\sigma$ in $L^1(\Omega)$ then

$$J(\delta\sigma) \leq \liminf_{k\rightarrow\infty} J(\delta\sigma_k),$$

i.e., the functional $J(\delta\sigma)$ is lower semicontinuous over $L^1(\Omega)$.

Proof. of Theorem 3.1. The proof follows the well-known direct method in the calculus of variations. Let $\{\delta\sigma_k\} \subset Y$ be a minimizing sequence for the functional J. We may assume that each $\delta\sigma_k$ is supported in the subdomain $\bar{\Omega}'$, for otherwise the function $\chi_{\Omega'}\delta\sigma_k$ still satisfies the constraint and we have $J(\chi_{\Omega'}\delta\sigma_k) \leq J(\delta\sigma_k)$. Then by the Sobolev-type inequality

$$\|\delta\sigma\|_{L^1(\Omega)} \leq C \int_\Omega |\nabla\delta\sigma|,$$

(see [11]), we can bound $\|\delta\sigma_k\|_{BV(\Omega)} \leq K$ for some constant K. It follows from Lemma 3.2 that there exists a subsequence (still denoted $\{\delta\sigma_k\}$), and a function $\delta\sigma \in L^1(\Omega)$ such that $\delta\sigma_k \rightarrow \delta\sigma$ in $L^1(\Omega)$. Clearly supp $\delta\sigma \subset \bar{\Omega}'$, so $\delta\sigma|_{\partial\Omega} = 0$. Since DF is continuous over $L^1(\Omega)$, we must have $\delta\sigma \in Y$. Finally, by the lower semicontinuity of J, we conclude that $\delta\sigma$ is in fact a minimizer of J. □

4. Stabilizing the constraints. There are two difficulties associated with the constraint $DF\ \delta\sigma = \delta g$. For the present time, let us view DF as an operator over $L^2(\Omega)$, and consider the following "near-null" subspace associated with DF:

$$V_{\text{near-null}} = \{v \ : \ v \in L^2(\Omega), \|DF\ v\| \leq \delta\},$$

for some small δ. The first difficulty is that if a measured data vector δg is not in the range of DF, we would never be able to satisfy the constraints. The second difficulty is that even if δg is in the range of DF, it is still possible for δg to have a component in the set $\{(DF\ v) \text{ where } v \in V_{\text{near-null}}\}$. When this happens, small changes in δg could lead to large changes in the subspace defined by the constraints $\{\delta\sigma \ : \ DF\ \delta\sigma = \delta g\}$.

We can take care of both difficulties by stabilizing the problem in the following way. Let δ be the "noise level" in the data. Consider the singular value decomposition (SVD):

$$DF = \mathbf{U}\Sigma\mathbf{V}^T,$$

where $\mathbf{U}$ is an $n^2 \times n^2$ orthogonal matrix, $\mathbf{V}$ is an orthogonal operator mapping $L^2(\Omega) \to L^2(\Omega)$, and Σ is a "diagonal" operator with diagonal $\{s_1, \ldots, s_{n^2}\}$, where $s_1 \geq s_2 \geq \ldots \geq s_{n^2}$. The diagonal entries of Σ are called the *singular values* of DF. Given any discrete approximation to $L^2(\Omega)$, the corresponding SVD of DF can be calculated numerically by standard methods, see [12]. A slightly different approach is needed if we choose not to discretize. Such an approach is outlined in [8].

Let s_p be the smallest singular value greater than δ. Form the new operators

$$\Sigma' = \text{diag}\{s_1, \ldots s_p\},$$

$$\mathbf{U}' = (\mathbf{u}_1, \ldots, \mathbf{u}_p),$$

and

$$\mathbf{V}' = (\mathbf{v}_1, \ldots, \mathbf{v}_p),$$

where $\mathbf{u}_j$ denotes the jth column of $\mathbf{U}$, and similarly for $\mathbf{v}_j$. Now we can form the "reduced rank" operator

$$M = \Sigma'\mathbf{V}'^T.$$

The range space of M is p-dimensional, and M has a well-defined pseudo-inverse $M^\dagger$ whose norm is less than or equal to $1/\delta$. The "stabilized" linear inverse problem can then be posed as

$$M\delta\sigma = \mathbf{U}'^T\delta g =: \delta g'.$$

The effect of this manipulation is that δg has been projected onto the subspace spanned by range vectors of DF whose singular values are greater than δ, thus eliminating both difficulties described above. Notice that the null space of the "reduced" operator M is exactly $V_{\text{near-null}}$. The constraint $M\delta\sigma = \delta g'$ defines a subspace of conductivity perturbations which are consistent with the observed data to within the noise level δ.

5. A minimization method. We can now formulate the minimal total variation reconstruction problem with stabilized linear constraints:

$$\min_{\delta\sigma \in X} J(\delta\sigma) = \int_\Omega |\nabla\delta\sigma|, \tag{16a}$$

$$\text{subject to } M\delta\sigma = \delta g', \tag{16b}$$

where $M : L^2(\Omega) \to \mathbb{R}^p$ is the linear operator constructed in the last section, and $X = \{\delta\sigma \in BV(\Omega) : \delta\sigma|_{\partial\Omega} = 0\}$. In the two-dimensional case we consider here, $BV(\Omega)$ imbeds in $L^2(\Omega)$, so the constraint makes sense, i.e., $M\delta\sigma$ is well-defined for $\delta\sigma \in BV(\Omega)$.

While it is possible to proceed from this point and attempt to solve problem (16) directly, the fact that the cost functional is not "smooth" creates certain complications

from both practical and theoretical standpoints. For this reason, our approach is to "mollify" the cost functional J with a small smoothing parameter and solve the resulting problem by straightforward methods. In principle the smoothing parameter can be taken arbitrarily small so that in the limit one should obtain a solution to problem (16). The problem we try to solve can be written

$$\min_{\delta\sigma \in X} J_\epsilon(\delta\sigma) = \int_\Omega h_\epsilon(|\nabla \delta\sigma|), \tag{17a}$$

$$\text{subject to } M\delta\sigma = \delta g', \tag{17b}$$

where

$$h_\epsilon(s) = \begin{cases} s & \text{if } s > \epsilon, \\ \frac{s^2}{2\epsilon} + \frac{\epsilon}{2} & \text{if } s \le \epsilon. \end{cases}$$

Thus h_ϵ is C^1 for $\epsilon > 0$. The effect of h_ϵ is to "round off" the corner in the absolute value function.

The following derivation is patterned after the approach taken by Rudin, Osher, and Fatemi in [14]. The Euler-Lagrange equations for problem (17) are formally given by

$$\nabla \cdot (q_\epsilon(|\nabla\delta\sigma|)\nabla\delta\sigma) - M^T\lambda = 0, \quad \text{in } \Omega, \tag{18a}$$

$$\delta\sigma = 0, \quad \text{on } \partial\Omega, \tag{18b}$$

$$M\delta\sigma = \delta g', \tag{18c}$$

where $\lambda \in I\!R^p$, M^T denotes the L^2 adjoint of M, and the function q_ϵ is defined by

$$q_\epsilon(s) = \frac{h_\epsilon'(s)}{s} = \begin{cases} 1/s & \text{if } s > \epsilon, \\ 1/\epsilon & \text{if } s \le \epsilon. \end{cases}$$

In [14] the approach to solving the Euler-Lagrange equations is to use time as an evolution (iteration) parameter. Applying this idea to our problem, we would solve

$$\delta\sigma_t = \nabla \cdot (q_\epsilon(|\nabla\delta\sigma|)\nabla\delta\sigma) - M^T\lambda, \quad \text{in } \Omega \times (0,\infty), \tag{19a}$$

$$\delta\sigma = 0, \quad \text{on } \partial\Omega \times (0,\infty), \tag{19b}$$

$$\delta\sigma(x,0) = \delta\sigma_0(x), \quad x \in \Omega, \tag{19c}$$

where $\delta\sigma_0$ is a solution of $M\delta\sigma_0 = \delta g'$, given, say, by the pseudo-inverse solution $\delta\sigma_0 = M^\dagger \delta g'$.

To solve the initial boundary value problem in (19), one could apply an explicit time-stepping scheme, that is, starting with the initial step $\delta\sigma_0$, apply the iteration

$$\delta\sigma_{i+1} = \delta\sigma_i + \tau\left[\nabla \cdot (q_\epsilon(|\nabla\delta\sigma_i|)\nabla\delta\sigma_i) - M^T\lambda^{(i)}\right], \tag{20}$$

where τ is the "step length". To solve for the Lagrange multiplier approximation $\lambda^{(i)}$, let $b_j \in L^2(\Omega)$ be a solution of

$$Mb_j = e_j, \quad j = 1, \ldots, p,$$

where e_j denotes the standard unit basis vectors for $I\!R^p$. Assuming that the SVD has already been calculated as in the last section, we can set $b_j = \mathbf{v}_j/s_j$, where $\mathbf{v}_j$ is the j-th column of the orthogonal operator $\mathbf{V}$. We see that if (18a) is satisfied then

$$\int_\Omega \nabla \cdot (q_\epsilon(|\nabla\delta\sigma|)\nabla\delta\sigma)b_j - \int_\Omega (M^T\lambda)b_j = 0,$$

and hence

$$\lambda_j = \langle \lambda, Mb_j \rangle = \int_\Omega (M^T\lambda) b_j = \int_\Omega \nabla \cdot (q_\epsilon(|\nabla \delta\sigma|)\nabla\delta\sigma) b_j. \tag{21}$$

One can calculate $\lambda^{(i)}$ directly from $\delta\sigma_i$ and the vectors b_j using equation (21). This procedure can be viewed as projecting the L^2 "gradient"

$$D_{\delta\sigma} J_\epsilon = -\nabla \cdot (q_\epsilon(|\nabla\delta\sigma|)\nabla\delta\sigma) \tag{22}$$

of the cost functional J_ϵ onto the linear subspace $\{\delta\sigma : M\delta\sigma = 0\}$. Thus, as pointed out in [14], the entire scheme can be viewed as a "projected gradient method".

Taking the viewpoint that the iteration scheme (20) is simply the projected gradient method, define the negative "projected gradient"

$$G_i = -D_{\delta\sigma} J_\epsilon(\delta\sigma_i) - M^T\lambda^{(i)}.$$

Our minimization procedure can be stated as follows.

1. Choose an initial steplength τ_0, a parameter $\epsilon > 0$, and an initial iterate $\delta\sigma_0$ satisfying the constraint (16b).
2. For $i = 1, \ldots,$ convergence do
3. If $J_\epsilon(\delta\sigma_i + \tau_i G_i) < J_\epsilon(\delta\sigma_i)$ then
   $\delta\sigma_{i+1} = \delta\sigma_i + \tau_i G_i$
   $\tau_{i+1} = \tau_i$
   else
   $\tau_i = \tau_i/2$
   If $\tau_i \|G_i\|$ is too small then stop
   otherwise go to step 3

end do

We note that our algorithm only has a provision for reducing the step size τ_i. A more complicated backtracking strategy that allows an increase as well as a decrease in the step size can be implemented. An earlier version of our code indeed uses such a strategy. We found that we *almost never* increase a step size during the iterations. While this is the case for our problem, it may not be true in general, and therefore, if one is to apply the method described here for other problems, it may be worthwhile to modify the algorithm to include the possibility of increasing the step size.

The computation of the projected gradient G_i above depends upon how we discretize the conductivity distribution $\delta\sigma$ and how we choose to approximate the partial differential operators. Rudin, et al [14] discretized their version of problem (19) directly (with $\epsilon = 0$), and used a rather sophisticated finite difference scheme to solve the evolution equation. Their time-stepping scheme, in the context of the projected gradient algorithm described above, is a fixed step-size version of our algorithm with a finite-difference approximation to the gradient $D_{\delta\sigma} J$. Their scheme does not check that the value of the "cost functional" is decreased at each step—the step size is restricted by a CFL condition.

Our approach to discretization is to begin by making the simplifying assumption that $\delta\sigma$ is a piecewise constant function over a square array of pixels. In this case, we can calculate the cost functional $J_\epsilon(\delta\sigma)$ in closed form. This leads to the further simplification that the gradient of $J_\epsilon(\delta\sigma)$ with respect to $\delta\sigma$ can be calculated exactly. This approach avoids the difficulty in choosing an appropriate finite difference approximation of the partial derivatives in G_i. An added bonus is that we have an

exact formula for the cost function $J_\epsilon(\delta\sigma_i)$ which we need in choosing the step size τ_i. Had a different discretization of $\delta\sigma$ been used, we may not have been able to compute $J_\epsilon(\delta\sigma)$ exactly, which would have lead to an added difficulty in testing the decrease in the value of J_ϵ at each iteration. A complete description of our implementation is presented in the next section.

In practice, we generally observed faster convergence for larger ϵ, but even so, the discretized scheme seems to converge even for very small positive values of ϵ.

To summarize the difference between our approach and that of Rudin et al, we might say that we view the problem primarily as an optimization problem, while Rudin, et al, view it primarily as a nonlinear diffusion problem. The advantages of our approach are: first, by standard theory we are guaranteed convergence for the discretized problem, and second, the step-length parameter τ is selected essentially automatically. Perhaps the main disadvantage to our approach is that we are not solving exactly the minimal total variation problem.

6. Implementation and numerical examples. Extending the domain Ω to the square

$$Q = (-1,1) \times (-1,1),$$

we discretize the conductivity perturbation $\delta\sigma$ to lie the space of piecewise constant functions on a uniform square grid with $N \times N$ cells. In this case $h_\epsilon(|\nabla\delta\sigma|)$ is a measure supported on the lines of the grid. Thus if we denote the value of $\delta\sigma$ on the (i,j)-th cell by $\delta\sigma_{i,j}$ then

$$\int_Q h_\epsilon(|\nabla\delta\sigma|) = \frac{1}{N}\sum_{i,j=1}^{N-1} h_\epsilon(|\delta\sigma_{i+1,j} - \delta\sigma_{i,j}|) + h_\epsilon(|\delta\sigma_{i,j+1} - \delta\sigma_{i,j}|).$$

Also discretizing the domain of the operator DF, the stabilized constraint operator M becomes a $p \times N^2$ matrix. From now on we denote the $\mathbb{R}^{N^2}$ vector $(\delta\sigma_{i,j})_{i,j=1}^N$ by $\delta\sigma$. Problem (17) can then be written

$$\min_{\delta\sigma\in X} J_\epsilon^N(\delta\sigma) = \frac{1}{N}\sum_{i,j=1}^{N-1} h_\epsilon(|\delta\sigma_{i+1,j} - \delta\sigma_{i,j}|) + h_\epsilon(|\delta\sigma_{i,j+1} - \delta\sigma_{i,j}|), \tag{23a}$$

$$\text{subject to } M\delta\sigma = \delta g', \tag{23b}$$

where X is the subset of $\mathbb{R}^{N^2}$ with zero "boundary values", that is,

$$X = \{\delta\sigma \in \mathbb{R}^{N^2} : \delta\sigma_{1,k} = \delta\sigma_{N,k} = \delta\sigma_{k,1} = \delta\sigma_{k,N} = 0, \quad k = 1,\ldots,N\}.$$

We can easily calculate the derivative of the functional $J(\delta\sigma)$. Since $\delta\sigma$ is really an $\mathbb{R}^{N^2}$-vector, this derivative is a gradient which is also in $\mathbb{R}^{N^2}$. Proceeding with the calculation, for $1 < k,l < N$, we find that

$$\begin{aligned}\frac{\partial J_\epsilon^N}{\partial\delta\sigma_{k,l}} &= q_\epsilon(|\delta\sigma_{k,l} - \delta\sigma_{k-1,l}|)(\delta\sigma_{k,l} - \delta\sigma_{k-1,l}) \\ &- q_\epsilon(|\delta\sigma_{k+1,l} - \delta\sigma_{k,l}|)(\delta\sigma_{k+1,l} - \delta\sigma_{k,l}) \\ &+ q_\epsilon(|\delta\sigma_{k,l} - \delta\sigma_{k,l-1}|)(\delta\sigma_{k,l} - \delta\sigma_{k,l-1}) \\ &- q_\epsilon(|\delta\sigma_{k,l+1} - \delta\sigma_{k,l}|)(\delta\sigma_{k,l+1} - \delta\sigma_{k,l})\,.\end{aligned} \tag{24}$$

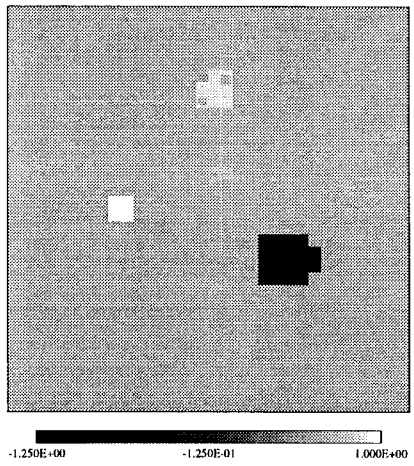

FIG. 1. *True profile for the first example.*

With the convention that $\partial J_\epsilon^N / \partial \delta\sigma_{k,l} = 0$ for k or l equal to 1 or N, these partial derivatives are the elements of the gradient of $J_\epsilon^N(\delta\sigma)$ over X:

$$\text{grad}_{\delta\sigma} J_\epsilon^N = \left(\frac{\partial J_\epsilon^N}{\partial \delta\sigma_{k,l}} \right)_{k,l=1}^{N}.$$

With this formula, we can easily compute the projected gradient G_i appearing in our minimization algorithm. We now have all the necessary ingredients to solve the problem (23).

In all of the following experiments we use a 32×32 grid. We further assume that the electrodes are point electrodes; i.e., the characteristic function χ in (2) is now a delta function. Moreover, we choose "dipole" current patterns so that f is a rotation of the vector $(1, -1, 0, \cdots, 0)^T$. The number of electrodes is fixed at 20 and we make 20 measurements, so the data vector δg consists of 400 data points. We remark that the method is certainly feasible for finer discretizations; most of the computational work in the problem is expended computing DF and its singular value decomposition. The data error tolerance is set at $\delta = 0.0001$, which resulted in 150 "usable" singular values in the SVD of DF. Thus the constraint operator M is a 150×1024 matrix and the reduced data vector $\delta g'$ has 150 elements. We took the smoothing parameter $\epsilon = 0.001$ for all experiments.

In the first experiment we attempt to recover the separated block profile pictured in Figure 1. The pseudo-inverse solution $\delta\sigma_0 = M^\dagger \, \delta g'$ was taken as the "initial guess" in the minimization procedure. The value of the cost functional $J_\epsilon^N(\delta\sigma_i)$ versus the number of iterations i is shown in Figure 2. Figure 3 compares the initial iterate $\delta\sigma_0$ with the final approximate minimizer. As the figure indicates, we obtain a near-exact reconstruction. It is interesting that the reconstruction not only sharpens the edges of the image, but also recovers nearly exactly the true values of the image on the "blocks".

Unfortunately it is not always possible to recover images as accurately as in the previous example. Roughly, since the reconstruction procedure favors "simple" images, if the original image is "complicated" (has large total variation), and most

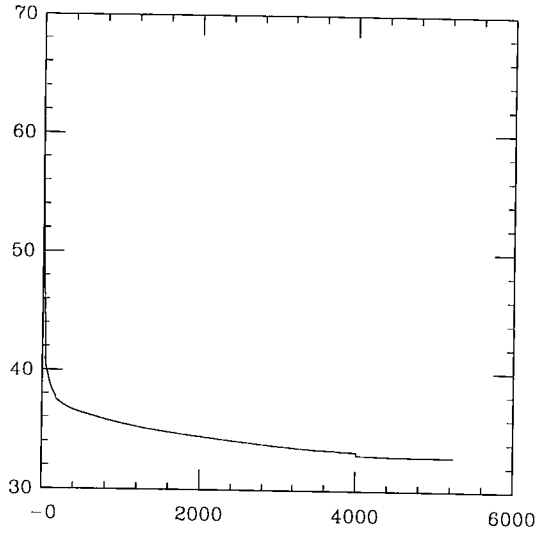

FIG. 2. *Functional value $J_\epsilon^N(\delta\sigma_i)$ versus iteration number i.*

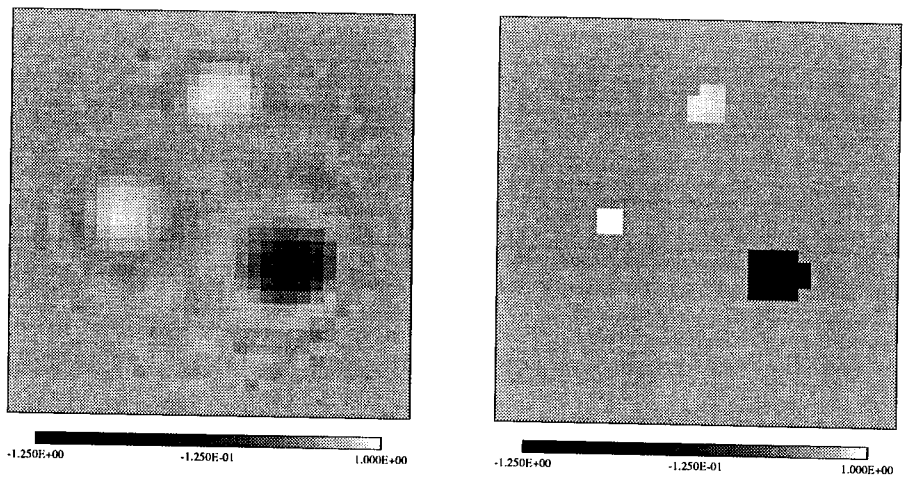

FIG. 3. *Comparison of pseudo-inverse solution and minimal total variation reconstruction for the first example. a.) Pseudo-inverse. b.) Reconstruction.*

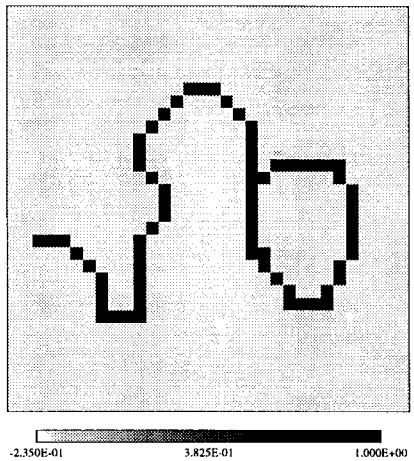

FIG. 4. *True profile for the second example.*

of the information about the variations of the image is lost in the measured data, then one should expect to obtain a reconstruction with less total variation than the original image. When this occurs the method has very little chance of success. This is illustrated in the following example. Figure 4 shows the true image consisting of a thin curved line. Figure 5 shows the comparison between the pseudo-inverse solution and the minimal total variation reconstruction. As it turns out, in this example the reconstruction has much lower total variation than the original image: approximately half as much. In fact, even the pseudo-inverse has less total variation than the original image in this example. Our impression after trying several such experiments is that the method generally has trouble recovering features such as thin lines. Presumably this is because (1) the line has large total variation compared to its "mass", and (2) too much information about the line is lost in the measured data. On the other hand, we observed that the method generally recovered quite accurately "blobs" such as those shown in the first example.

The preceding two examples were designed to illustrate the extremes one can observe in the accuracy of the reconstructions. For the last example, we will try to indicate the behavior of the method in a somewhat more realistic situation. A caricature of a cross-section of the human torso is pictured in Figure 6. The large light-colored areas on the right and left indicate the lungs, the slightly darker area between the lungs represents muscle and other tissue, and the two dark areas in the lower center represent heart chambers filled with blood. Many details have been omitted from the image, of course. Since we are solving the linearized problem, one might think of Figure 6 as the *difference* between the true image and some background conductivity.

As can be seen from Figure 7, the reconstruction recovers some features not visible in the pseudo-inverse, most noticeably the lungs and the tissue between the lungs. In this example as in the previous example, the reconstruction had lower total variation than the original image (approximately 50 vs. 66), however in this case the pseudo-inverse had higher total variation (approximately 76).

We have also investigated the effects of noise in the data on the reconstruction. The stabilization procedure outlined in Section 4 can be adjusted to the noise level

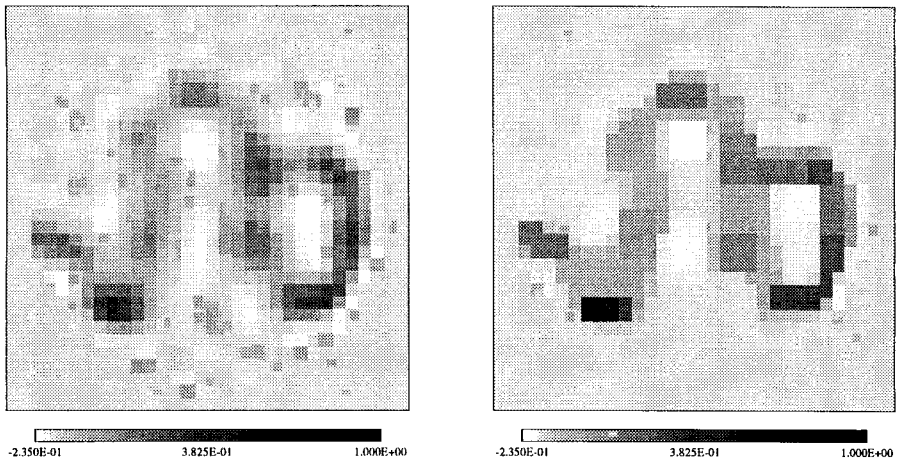

FIG. 5. *Comparison of pseudo-inverse solution and minimal total variation reconstruction for the second example. a.) Pseudo-inverse. b.) Reconstruction.*

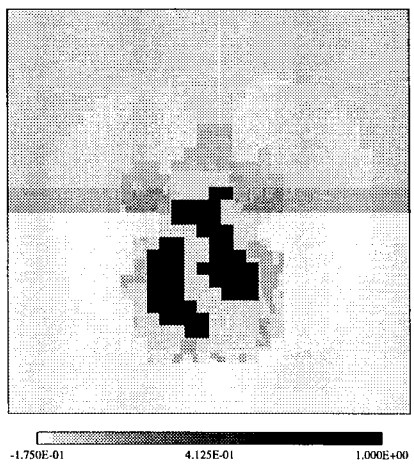

FIG. 6. *True profile for the third example.*

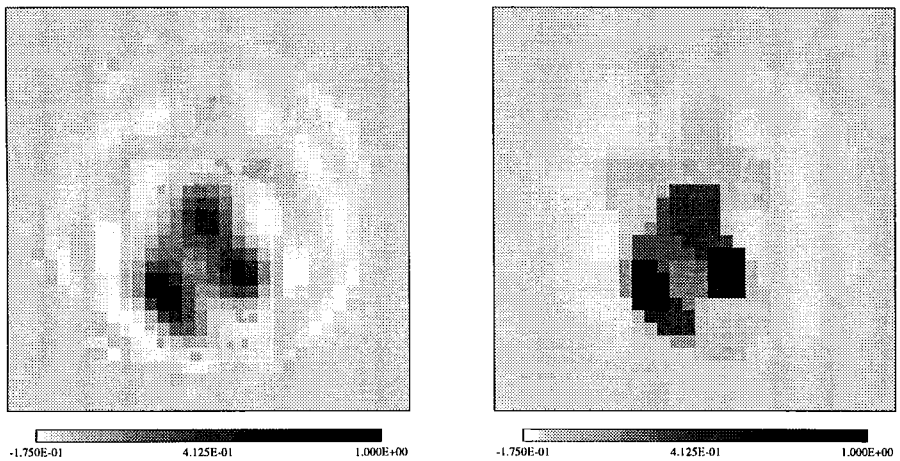

FIG. 7. *Comparison of pseudo-inverse solution and minimal total variation reconstruction for the third example. a.) Pseudo-inverse. b.) Reconstruction.*

by changing the value of δ. Noise was added by taking a "clean" data set and adding random numbers of less than a prescribed value. We found that noise has little effect on problems for which the method works well; e.g., Examples 1 and 3. The effect of noise did not worsen the reconstructions on problems that the method had difficulty with, such as Example 2. While these simulations gave us some confidence that the method has a hope of performing well on real data, we feel that we need to gain more experience with the method, especially for the full nonlinear problem, before using it to invert experimental data.

7. Directions for future research. From the preliminary results we have presented so far, we believe that the idea of using image enhancing techniques in electrical impedance tomography is quite promising. In addition, the problem poses some interesting questions that require further investigation.

In the work presented here, we have considered the linearized problem. Of course, the real problem we need to solve is nonlinear. Applying the image enhancement strategy for the full nonlinear problem would require the solution of the following minimization

$$\min_{\sigma \in X} J(\delta\sigma) = \int_\Omega |\nabla \delta\sigma|, \tag{25a}$$

$$\text{subject to } F(\sigma, f^{(i)}) = g^{(i)}, \quad i = 1 \ldots n. \tag{25b}$$

Please refer to Section 2 for a description of $F(\sigma, f^{(i)})$ and $g^{(i)}$. The notable difference in the problem above is that the constraint is nonlinear, and the feasible set will be, as in the linear case, sensitive to data errors. A natural approach is to put the constraints as a penalty term. Such an approach has been considered in different contexts in [16] and [7].

Another problem that requires attention is the method for minimization. The approach taken here, which is related to a projected gradient method, is clearly inefficient. This can be seen by the decrease of the cost function as a function of iteration in Figure 2. The main difficulty in doing the minimization stems from the fact that

the original cost function is not everywhere differentiable. There are, however, optimization methods that are designed to tackle just such cost functions [5]. We plan to look into applying such methods to our minimization problem.

Using the discretization of the conductivity in Section 6, we arrive at a problem of determining a function which is piecewise constant on an array of square pixels, that is "blocky". It seems that the "blockiness" attribute can be described efficiently using the Haar basis. This claim is based on the observation that "blocky" functions have separated scales. It is quite possible that by using the Haar basis to represent the unknown conductivity, an efficient minimization can be constructed.

A last, and perhaps most difficult problem, has to do with the development of an uncertainty principle for this problem. That is, given that the conductivity we wish to reconstruct is "blocky" and has a given BV-norm, how much data are required to uniquely reconstruct it using the minimal variation approach? A discrete version of such a principle seems possible. For convolution problems in 1-D, discrete and continuous, facts like this have been established [9, 15].

Acknowledgements. The authors are pleased to acknowledge very fruitful correspondence on this work with Professor Robert Kohn. We also thank Professor Avner Friedman for several helpful suggestions and references. This work was begun while the second author (FS) was visiting the Institute for Mathematics and its Applications in the Fall of 1992.

REFERENCES

[1] A. Allers and F. Santosa, *Stability and resolution analysis of a linearized problem in electrical impedance tomography*, Inverse Problems, 7 (1991), pp. 515–533.

[2] L. Alvarez, P. Lions, and J. Morel, *Image selective smoothing and edge detection by nonlinear diffusion*, SIAM J. Numer. Anal., (1993), p. to appear.

[3] D. Barber, B. Brown, and J. Jossinet, *Electrical impedance tomography*, Clinical Physics and Physiological Measurements, 9 (1988). Supplement A.

[4] F. Catté, P. Lions, J. Morel, and T. Coll, *Image selective smoothing and edge detection by nonlinear diffusion*, SIAM J. Numer. Anal., 29 (1992), pp. 182–193.

[5] T. Coleman and Y. Li, *A globally and quadratically convergent affine scaling method for linear l_1 problems*, Mathematical Programming, 56 (1992), pp. 189–222.

[6] D. Dobson, *Estimates on resolution and stabilization for the linearized inverse conductivity problem*, Inverse Problems, 8 (1992), pp. 71–81.

[7] ———, *Exploiting ill-posedness in the design of diffractive optical structures*, in Mathematics in Smart Structures, H. Banks, ed., SPIE, 1993. to appear.

[8] D. Dobson and F. Santosa, *Stability and resolution analysis of an inverse problem in electical impedance tomography – dependence on the input current patterns.* to appear in SIAM J. Appl. Math, IMA Preprint No. 1038.

[9] D. Donoho, *Superresolution via sparsity constraints*, SIAM J. Math. Anal., 23 (1992), pp. 1309–1331.

[10] D. Gilbarg and N. Trudinger, *Elliptic Partial Differential Equations of Second Order*, Springer–Verlag, Berlin, 1983. Second edition.

[11] E. Giusti, *Minimal Surfaces and Functions of Bounded Variation*, Birkhauser, Boston, 1984. Monographs in Mathematics, Vol. 80.

[12] G. Golub and C. V. Loan, *Matrix Computations*, Johns Hopkins, 1983.

[13] L. Rudin and S. Osher, *Feature-oriented image enhancement using shock filters*, SIAM J. Numer. Anal., 27 (1990), pp. 919–940.

[14] L. Rudin, S. Osher, and E. Fatemi, *Nonlinear total variation based noise removal algorithms*, Physica D. to appear.

[15] F. Santosa and W. Symes, *Linear inversion of band-limited reflection seismograms*, SIAM J. Sci. Stat. Comput., 7 (1986), pp. 1307–1330.

[16] ———, *Reconstruction of blocky impedance profiles from normal-incidence reflection seismograms which are band-limited and miscalibrated*, Wave Motion, 10 (1988), pp. 209–230.

#	Author/s	Title
1063	**Eduardo Casas & Jiongmin Yong**	Maximum principle for state-constrained optimal control problems governed by quasilinear elliptic equations
1064	**Suzanne M. Lenhart & Jiongmin Yong**	Optimal control for degenerate parabolic equations with logistic growth
1065	**Suzanne Lenhart**	Optimal control of a convective-diffusive fluid problem
1066	**Enrique Zuazua**	Weakly nonlinear large time behavior in scalar convection-diffusion equations
1067	**Caroline Fabre, Jean-Pierre Puel & Enrike Zuazua**	Approximate controllability of the semilinear heat equation
1068	**M. Escobedo, J.L. Vazquez & Enrike Zuazua**	Entropy solutions for diffusion-convection equations with partial diffusivity
1069	**M. Escobedo, J.L. Vazquez & Enrike Zuazua**	A diffusion-convection equation in several space dimensions
1070	**F. Fagnani & J.C. Willems**	Symmetries of differential systems
1071	**Zhangxin Chen, Bernardo Cockburn, Joseph W. Jerome & Chi-Wang Shu**	Mixed-RKDG finite element methods for the 2-D hydrodynamic model for semiconductor device simulation
1072	**M.E. Bradley & Suzanne Lenhart**	Bilinear optimal control of a Kirchhoff plate
1073	**Héctor J. Sussmann**	A cornucopia of abnormal subriemannian minimizers. Part I: The four-dimensional case
1074	**Marek Rakowski**	Transfer function approach to disturbance decoupling problem
1075	**Yuncheng You**	Optimal control of Ginzburg-Landau equation for superconductivity
1076	**Yuncheng You**	Global dynamics of dissipative modified Korteweg-de Vries equations
1077	**Mario Taboada & Yuncheng You**	Nonuniformly attracting inertial manifolds and stabilization of beam equations with structural and Balakrishnan-Taylor damping
1078	**Michael Böhm & Mario Taboada**	Global existence and regularity of solutions of the nonlinear string equation
1079	**Zhangxin Chen**	BDM mixed methods for a nonlinear elliptic problem
1080	**J.J.L. Velázquez**	On the dynamics of a closed thermosyphon
1081	**Frédéric Bonnans & Eduardo Casas**	Some stability concepts and their applications in optimal control problems
1082	**Hong-Ming Yin**	$\mathcal{L}^{2,\mu}(Q)$-estimates for parabolic equations and applications
1083	**David L. Russell & Bing-Yu Zhang**	Smoothing and decay properties of solutions of the Korteweg-de Vries equation on a periodic domain with point dissipation
1084	**J.E. Dunn & K.R. Rajagopal**	Fluids of differential type: Critical review and thermodynamic analysis
1085	**Mary Elizabeth Bradley & Mary Ann Horn**	Global stabilization of the von Kármán plate with boundary feedback acting via bending moments only
1086	**Mary Ann Horn & Irena Lasiecka**	Global stabilization of a dynamic von Kármán plate with nonlinear boundary feedback
1087	**Vilmos Komornik**	Decay estimates for a petrovski system with a nonlinear distributed feedback
1088	**Jesse L. Barlow**	Perturbation results for nearly uncoupled Markov chains with applications to iterative methods
1089	**Jong-Shenq Guo**	Large time behavior of solutions of a fast diffusion equation with source
1090	**Tongwen Chen & Li Qiu**	$\mathcal{H}_\infty$ design of general multirate sampled-data control systems
1091	**Satyanad Kichenassamy & Walter Littman**	Blow-up surfaces for nonlinear wave equations, I
1092	**Nahum Shimkin**	Asymptotically efficient adaptive strategies in repeated games, Part I: certainty equivalence strategies
1093	**Caroline Fabre, Jean-Pierre Puel & Enrique Zuazua**	On the density of the range of the semigroup for semilinear heat equations
1094	**Robert F. Stengel, Laura R. Ray & Christopher I. Marrison**	Probabilistic evaluation of control system robustness
1095	**H.O. Fattorini & S.S. Sritharan**	Optimal chattering controls for viscous flow
1096	**Kathryn E. Lenz**	Properties of certain optimal weighted sensitivity and weighted mixed sensitivity designs
1097	**Gang Bao & David C. Dobson**	Second harmonic generation in nonlinear optical films
1098	**Avner Friedman & Chaocheng Huang**	Diffusion in network
1099	**Xinfu Chen, Avner Friedman & Tsuyoshi Kimura**	Nonstationary filtration in partially saturated porous media
1100	**Walter Littman & Baisheng Yan**	Rellich type decay theorems for equations $P(D)u = f$ with f having support in a cylinder
1101	**Satyanad Kichenassamy & Walter Littman**	Blow-up surfaces for nonlinear wave equations, II
1102	**Nahum Shimkin**	Extremal large deviations in controlled I.I.D. processes with applications to hypothesis testing
1103	**A. Narain**	Interfacial shear modeling and flow predictions for internal flows of pure vapor experiencing film condensation
1104	**Andrew Teel & Laurent Praly**	Global stabilizability and observability imply semi-global stabilizability by output feedback
1105	**Karen Rudie & Jan C. Willems**	The computational complexity of decentralized discrete-event control problems

1106 **John A. Burns & Ruben D. Spies**, A numerical study of parameter sensitivities in Landau-Ginzburg models of phase transitions in shape memory alloys

1107 **Gang Bao & William W. Symes**, Time like trace regularity of the wave equation with a nonsmooth principal part

1108 **Lawrence Markus**, A brief history of control

1109 **Richard A. Brualdi, Keith L. Chavey & Bryan L. Shader**, Bipartite graphs and inverse sign patterns of strong sign-nonsingular matrices

1110 **A. Kersch, W. Morokoff & A. Schuster**, Radiative heat transfer with quasi-monte carlo methods

1111 **Jianhua Zhang**, A free boundary problem arising from swelling-controlled release processes

1112 **Walter Littman & Stephen Taylor**, Local smoothing and energy decay for a semi-infinite beam pinned at several points and applications to boundary control

1113 **Srdjan Stojanovic & Thomas Svobodny**, A free boundary problem for the Stokes equation via nonsmooth analysis

1114 **Bronislaw Jakubczyk**, Filtered differential algebras are complete invariants of static feedback

1115 **Boris Mordukhovich**, Discrete approximations and refined Euler-Lagrange conditions for nonconvex differential inclusions

1116 **Bei Hu & Hong-Ming Yin**, The profile near blowup time for solution of the heat equation with a nonlinear boundary condition

1117 **Jin Ma & Jiongmin Yong**, Solvability of forward-backward SDEs and the nodal set of Hamilton-Jacobi-Bellman Equations

1118 **Chaocheng Huang & Jiongmin Yong**, Coupled parabolic and hyperbolic equations modeling age-dependent epidemic dynamics with nonlinear diffusion

1119 **Jiongmin Yong**, Necessary conditions for minimax control problems of second order elliptic partial differential equations

1120 **Eitan Altman & Nahum Shimkin**, Worst-case and Nash routing policies in parallel queues with uncertain service allocations

1121 **Nahum Shimkin & Adam Shwartz**, Asymptotically efficient adaptive strategies in repeated games, part II: Asymptotic optimality

1122 **M.E. Bradley**, Well-posedness and regularity results for a dynamic Von Kármán plate

1123 **Zhangxin Chen**, Finite element analysis of the 1D full drift diffusion semiconductor model

1124 **Gang Bao & David C. Dobson**, Diffractive optics in nonlinear media with periodic structure

1125 **Steven Cox & Enrique Zuazua**, The rate at which energy decays in a damped string

1126 **Anthony W. Leung**, Optimal control for nonlinear systems of partial differential equations related to ecology

1127 **H.J. Sussmann**, A continuation method for nonholonomic path-finding problems

1128 **Yung-Jen Guo & Walter Littman**, The null boundary controllability for semilinear heat equations

1129 **Q. Zhang & G. Yin**, Turnpike sets in stochastic manufacturing systems with finite time horizon

1130 **I. Györi, F. Hartung & J. Turi**, Approximation of functional differential equations with time- and state-dependent delays by equations with piecewise constant arguments

1131 **I. Györi, F. Hartung & J. Turi**, Stability in delay equations with perturbed time lags

1132 **F. Hartung & J. Turi**, On the asymptotic behavior of the solutions of a state-dependent delay equation

1133 **Pierre-Alain Gremaud**, Numerical optimization and quasiconvexity

1134 **Jie Tai Yu**, Resultants and inversion formula for N polynomials in N variables

1135 **Avner Friedman & J.L. Velázquez**, The analysis of coating flows in a strip

1136 **Eduardo D. Sontag**, Control of systems without drift via generic loops

1137 **Yuan Wang & Eduardo D. Sontag**, Orders of input/output differential equations and state space dimensions

1138 **Scott W. Hansen**, Boundary control of a one-dimensional, lienar, thermoelastic rod

1139 **Robert Lipton & Bogdan Vernescu**, Homogenization of two phase emulsions with surface tension effects

1140 **Scott Hansen & Enrique Zuazua**, Exact controllability and stabilization of a vibrating string with an interior point mass

1141 **Bei Hu & Jiongmin Yong**, Pontryagin Maximum principle for semilinear and quasilinear parabolic equations with pointwise state constraints

1142 **Mark H.A. Davis**, A deterministic approach to optimal stopping with application to a prophet inequality

1143 **M.H.A. Davis & M. Zervos**, A problem of singular stochastic control with discretionary stopping

1144 **Bernardo Cockburn & Pierre-Alain Gremaud**, An error estimate for finite element methods for scalar conservation laws

1145 **David C. Dobson & Fadil Santosa**, An image enhancement technique for electrical impedance tomography

1146 **Jin Ma, Philip Protter, & Jiongmin Yong**, Solving forward-backward stochastic differential equations explicitly — a four step scheme

1147 **Yong Liu**, The equilibrium plasma subject to skin effect

1148 **Ulrich Hornung**, Models for flow and transport through porous media derived by homogenization

1149 **Avner Friedman, Chaocheng Huang, & Jiongmin Yong**, Effective permeability of the boundary of a domain

1150 **Gang Bao**, A uniqueness theorem for an inverse problem in periodic diffractive optics

1151 **Angelo Favini, Mary Ann Horn,& Irena Lasiecka**, Global existence and uniqueness of regular solutions to the dynamic von Kármán system with nonlinear boundary dissipation